PROCEEDINGS of the
23rd International Congress on Acoustics

9 to 13 September 2019 in Aachen, Germany

3-D numerical simulation of nonlinear elastic wave propagation in locally damaged materials

Benjamin ANKAY[1]; Chuanzeng ZHANG[1]

[1]Chair of Structural Mechanics, University of Siegen, D-57068 Siegen, Germany

ABSTRACT

In this paper, the three-dimensional (3-D) ultrasonic wave propagation problem in an elastic half-space with a localized damage zone is numerically simulated by a mapped staggered Chebyshev pseudo-spectral method. To simulate the semi-infinite elastic half-space, convolutional perfectly matched layers (CPMLs) are implemented on the artificial boundaries of the half-space. Classical nonlinear elastic and non-classical hysteretic material laws are used to consider the localized damage zone within the half-space. In particular, the nonlinear wave scattering problem is investigated by applying a frequency-domain analysis. Based on the numerical results, the main properties of the scattered harmonic wave fields are revealed and compared with analytical solutions.

Keywords: Nonlinear wave propagation, Chebyshev pseudo-spectral collocation method, Nonlinear elastic wave scattering

1. INTRODUCTION

The study of the nonlinear wave propagation problems can be traced back to the early works of Murnaghan (1), Truesdell and Toupin (2), Landau and Lifshitz (3) et al. In these works, the nonlinear elastic constitutive equations for a general 3-D continuum have been derived by expanding the strain energy into additional higher-order elastic terms (physically nonlinear) and applying a finite strain theory (geometrically nonlinear). This classical nonlinear elastic theory can describe the nonlinear properties of homogeneous materials sufficiently well. However, considering heterogeneous or damaged materials, the classical nonlinear elastic theory is often insufficient to describe the essential elastodynamic and acoustic phenomena (4, 5). Due to this fact, additional material models have been developed in recent decades that extend or complement the classical nonlinear elastic theory. In contrast to the classical nonlinear elastic theory, several material models have been proposed in the framework of the non-classical nonlinear elastic theory (6, 7). Generally speaking, ultrasonic testing methods based on the nonlinear elastic theory can be used to investigate especially the nonlinear elastic material properties. Besides, ultrasonic experiments, where the wave velocity change in a nonlinear elastic medium during static or dynamic loading is analyzed (8-11), the so-called finite-amplitude ultrasonic methods (12, 13) have proven to be a promising nondestructive testing technique for early damage detection. The sensitivity of this method to microstructural changes and damages is considerably higher than the conventional method based on linear ultrasonic waves (14). Usually, such nonlinear ultrasonic experiments are based on an evaluation of the higher-order harmonics in the frequency spectrum of the corresponding ultrasonic signals (12, 13). In the past years, this method has already been applied successfully for assessing the damage states in different engineering materials (15-18). By choosing an appropriate acoustic nonlinearity parameter (ANLP) the damage progress attributed to micro-cracking, dislocations, corrosion or thermal loading can be evaluated. Furthermore, numerous advanced ultrasonic methods have been developed that are based on the wave mixing technique (19). In addition to the analytical and experimental investigations, wave propagation problems in a nonlinear elastic medium have been also performed extensively by numerical simulations (20, 21). In most investigated cases, the respective nonlinearity was assumed to be homogeneously distributed over the entire physical domain. However, due to the heterogeneity of the microstructures and the non-uniform stress distributions early damages often initiate in a localized

[1] ankay@bau.uni-siegen.de

region inside the structure. Therefore, to describe and localize the real damage progress in more detail, it is important to analyze the processes and interactions of the elastic wave propagation in localized damaged structures. In recent years, some studies have already examined this specific problem analytically (22-24). In these previous works, a spherical nonlinear elastic inclusion within an undamaged linear elastic host medium has been considered as the damage zone, and the analytical expressions for the scattered harmonic wave fields have been derived using the scattered far-field solutions. Depending on the wavelength, the radius of the inclusion and the elastic wave mode (longitudinal or shear wave), a characteristic distribution or shape of the associated scattered wave field exists. Based on the above-mentioned analytical solutions, the wave propagation problem in a 3-D isotropic, linear elastic medium with a spherical nonlinear elastic region will be numerically investigated in this study. In addition to the case of a quadratic nonlinear elastic inclusion, a hysteretic nonlinear elastic inclusion is also analyzed by applying a suitable material law. Subsequently, the numerical results for the two cases will be compared and discussed in the context of the analytical solutions.

2. NONLINEAR ELASTICITY

2.1 Classical quadratic nonlinear elasticity

Considering the third-order terms in the elastic strain energy of an isotropic solid the following expression can be obtained

$$\phi = \frac{\lambda + 2\mu}{2} I_1^2 - 2\mu I_2 + \frac{l + 2m}{3} I_1^3 - 2m I_1 I_2 + n I_3 \tag{1}$$

Here, ϕ is the elastic strain energy, λ and μ are the second-order elastic constants, l, m and n are the third-order elastic constants according to Murnaghan (1), and I_1, I_2 and I_3 represent the invariants of the strain tensor. By assuming infinitesimal strains and neglecting nonlinear contributions in the strain tensor, the strain invariants in Eq. (1) can be expressed as follows

$$\begin{aligned} I_1 &= \varepsilon_x + \varepsilon_y + \varepsilon_z, \\ I_2 &= (\varepsilon_x \varepsilon_y + \varepsilon_y \varepsilon_z + \varepsilon_z \varepsilon_x) - \tfrac{1}{4}\left(\gamma_{xy}^2 + \gamma_{yz}^2 + \gamma_{xy}^2\right), \\ I_3 &= \varepsilon_x \varepsilon_y \varepsilon_z + \tfrac{1}{4}\gamma_{xy}\gamma_{yz}\gamma_{xz} - \varepsilon_x \gamma_{yz}^2 - \varepsilon_y \gamma_{xz}^2 - \varepsilon_z \gamma_{xy}^2, \end{aligned} \tag{2}$$

where the infinitesimal strains are defined by

$$\varepsilon_x = \frac{\partial u}{\partial x},\ \varepsilon_y = \frac{\partial v}{\partial y},\ \varepsilon_z = \frac{\partial w}{\partial z},\ \gamma_{xy} = \left(\frac{\partial u}{\partial y} + \frac{\partial v}{\partial x}\right),\ \gamma_{yz} = \left(\frac{\partial v}{\partial z} + \frac{\partial w}{\partial y}\right),\ \gamma_{xz} = \left(\frac{\partial w}{\partial x} + \frac{\partial u}{\partial z}\right). \tag{3}$$

Here, u, v and w denote the displacements of the 3-D continuum in the x-, y- and z-directions. Differentiating the strain energy given by Eq. (1) with respect to the strains defined by Eq. (3) yields the following normal and shear stresses

$$\begin{aligned} \sigma_x &= E_1\varepsilon_x + \lambda\left(\varepsilon_y + \varepsilon_z\right) + E_2\varepsilon_x^2 + l\left(\varepsilon_y^2 + \varepsilon_z^2\right) + 2l\varepsilon_x\left(\varepsilon_y + \varepsilon_z\right) + \left(2(l-m) + n\right)\varepsilon_y\varepsilon_z + \frac{m}{2}\left(\gamma_{xy}^2 + \gamma_{yz}^2 + \gamma_{xz}^2\right) - \frac{n}{4}\gamma_{yz}^2, \\ \sigma_y &= E_1\varepsilon_y + \lambda\left(\varepsilon_x + \varepsilon_z\right) + E_2\varepsilon_y^2 + l\left(\varepsilon_x^2 + \varepsilon_z^2\right) + 2l\varepsilon_y\left(\varepsilon_x + \varepsilon_z\right) + \left(2(l-m) + n\right)\varepsilon_x\varepsilon_z + \frac{m}{2}\left(\gamma_{xy}^2 + \gamma_{yz}^2 + \gamma_{xz}^2\right) - \frac{n}{4}\gamma_{xz}^2, \\ \sigma_z &= E_1\varepsilon_z + \lambda\left(\varepsilon_x + \varepsilon_y\right) + E_2\varepsilon_z^2 + l\left(\varepsilon_x^2 + \varepsilon_y^2\right) + 2l\varepsilon_z\left(\varepsilon_x + \varepsilon_y\right) + \left(2(l-m) + n\right)\varepsilon_x\varepsilon_y + \frac{m}{2}\left(\gamma_{xy}^2 + \gamma_{yz}^2 + \gamma_{xz}^2\right) - \frac{n}{4}\gamma_{xy}^2, \end{aligned} \tag{4}$$

$$\begin{aligned} \tau_{xy} &= \mu\gamma_{xy} + m\gamma_{xy}\left(\varepsilon_x + \varepsilon_y + \varepsilon_z\right) + \frac{n}{4}\left(\gamma_{xz}\gamma_{yz} - 2\varepsilon_z\gamma_{xy}\right), \\ \tau_{xz} &= \mu\gamma_{xz} + m\gamma_{xz}\left(\varepsilon_x + \varepsilon_y + \varepsilon_z\right) + \frac{n}{4}\left(\gamma_{xy}\gamma_{yz} - 2\varepsilon_y\gamma_{xz}\right), \\ \tau_{yz} &= \mu\gamma_{yz} + m\gamma_{yz}\left(\varepsilon_x + \varepsilon_y + \varepsilon_z\right) + \frac{n}{4}\left(\gamma_{xy}\gamma_{xz} - 2\varepsilon_x\gamma_{yz}\right), \end{aligned} \tag{5}$$

with $E_1 = \lambda + 2\mu$ and $E_2 = l + 2m$.

2.2 Hysteretic nonlinear elasticity

As already mentioned in the introduction, that for an appropriate description of the nonlinear elastic behavior of many engineering materials, it is often not sufficient to apply only the classical nonlinear elastic theory. Therefore, non-classical nonlinear elastic theory has to be applied. Especially in heterogeneous materials, such as concretes, composites and damaged structures, a pronounced non-classical hysteretic material behavior is often observed. To model the hysteretic nonlinear behavior, the Nazarov-hysteresis model (25) is used in this study. In this case, the 1-D governing constitutive equation is given by

$$\sigma_x = E_1\left(\varepsilon_x - f\left(\varepsilon_x, \dot{\varepsilon}_x\right)\right), \tag{6}$$

where for the purely elastic case we have

$$f\left(\varepsilon, \dot{\varepsilon}\right) = \frac{1}{n_N}\begin{cases} \gamma_1 \varepsilon^{n_N}, & \varepsilon > 0,\ \dot{\varepsilon} > 0, \\ -\gamma_2 \varepsilon^{n_N} + \left(\gamma_1 + \gamma_2\right)\varepsilon_{m+}^{n_N - 1}\varepsilon, & \varepsilon > 0,\ \dot{\varepsilon} < 0, \\ -\gamma_3 \varepsilon^{n_N}, & \varepsilon < 0,\ \dot{\varepsilon} < 0, \\ \gamma_4 \varepsilon^{n_N} - \left(\gamma_3 + \gamma_4\right)\varepsilon_{m-}^{n_N - 1}\varepsilon, & \varepsilon > 0,\ \dot{\varepsilon} < 0, \end{cases} \tag{7}$$

with the hysteretic material parameters $\gamma_1 - \gamma_4$ and the exponent n_N. In Eq. (7), ε_{m+} and ε_{m-} denote the maximum and minimum strains in the current hysteresis loop. To transform the 1-D constitutive equations to 3-D, the Kelvin decomposition method (26, 27) is used. Here, the linear elastic stiffness matrix in the Voigt notation $\mathbf{C}^V$ is transformed to the Kelvin notation $\mathbf{C}^K$ by applying the transformation relation $\mathbf{C}^K = \mathbf{T}\mathbf{C}^V\mathbf{T}$, where the corresponding transformation matrix is defined by

$$\mathbf{T} = \mathrm{diag}\left(1,\ 1,\ 1,\ \sqrt{2},\ \sqrt{2},\ \sqrt{2}\right). \tag{8}$$

Accordingly, the corresponding strain and stress vectors can be defined by $\boldsymbol{\varepsilon}^K = \left(\varepsilon_x, \varepsilon_y, \varepsilon_z, \sqrt{2}\varepsilon_{xy}, \sqrt{2}\varepsilon_{xz}, \sqrt{2}\varepsilon_{yz}\right)$ and $\boldsymbol{\sigma}^K = \left(\sigma_x, \sigma_y, \sigma_z, \sqrt{2}\tau_{xy}, \sqrt{2}\tau_{xz}, \sqrt{2}\tau_{yz}\right)$. Subsequently, the eigenvalue problem of the Kelvin system is solved to obtain the respective constitutive relations in the eigensystem as $\hat{\boldsymbol{\sigma}} = \hat{\mathbf{C}}\hat{\boldsymbol{\varepsilon}}$. For an isotropic linear elastic solid, the so-called eigenstiffness matrix can be obtained via the corresponding eigenvalues as follows

$$\hat{\mathbf{C}} = diag\left(\left[3\lambda + 2\mu,\ 2\mu,\ 2\mu,\ \mu,\ \mu,\ \mu\right]\right). \tag{9}$$

By means of the eigenvectors, the so-called eigenstrains or eigenstresses are defined by

$$\begin{aligned} \hat{\boldsymbol{\sigma}} &= \left[\hat{\sigma}_1, \hat{\sigma}_2, \hat{\sigma}_3, \hat{\tau}_1, \hat{\tau}_2, \hat{\tau}_3\right] = \left[\tfrac{1}{\sqrt{3}}\left(\sigma_x + \sigma_y + \sigma_z\right),\ \tfrac{1}{\sqrt{6}}\left(2\sigma_z - \sigma_x - \sigma_y\right),\ \tfrac{1}{\sqrt{2}}\left(\sigma_y - \sigma_x\right),\ \tau_{xy},\ \tau_{xz},\ \tau_{yz}\right]^T, \\ \hat{\boldsymbol{\varepsilon}} &= \left[\hat{\varepsilon}_1, \hat{\varepsilon}_2, \hat{\varepsilon}_3, \hat{\gamma}_1, \hat{\gamma}_2, \hat{\gamma}_3\right] = \left[\tfrac{1}{\sqrt{3}}\left(\varepsilon_x + \varepsilon_y + \varepsilon_z\right),\ \tfrac{1}{\sqrt{6}}\left(2\varepsilon_z - \varepsilon_x - \varepsilon_y\right),\ \tfrac{1}{\sqrt{2}}\left(\varepsilon_y - \varepsilon_x\right),\ \gamma_{xy},\ \gamma_{xz},\ \gamma_{yz}\right]^T. \end{aligned} \tag{10}$$

In the obtained system of equations, the associated eigenstresses are independent of each other and detached from the original coordinate system. Thus, when it is stretched in one particular eigenstress direction, no elastic energy is effectively involved in the other stress directions (invariant system) (27). Therefore, the scalar hysteretic nonlinear stress-strain relationships can be applied for each of the six independent directions. Finally, the stress components in the original Cartesian coordinate system can be obtained by the inverse transform.

3. STAGGERED CHEBYSHEV-PSEUDOSPECTRAL COLLOCATION METHOD

Due to the advantages of the spectral methods regarding computing time and memory requirement, a numerical collocation method based on the Chebyshev polynomials is applied in this study. This method has already been developed several decades ago (28) and has been successfully applied in the fields of engineering, geoscience or meteorology. In contrast to the Fourier spectral methods it can also be applied to non-periodic boundary value problems. In the following, the key steps of the present numerical method and the corresponding modifications are briefly explained. Firstly, the governing

equations of motion for the 3-D wave propagation problems are recast into a first-order hyperbolic system of partial differential equations (PDEs), which can be written in the following form

$$\frac{\partial v_x}{\partial t}=\frac{1}{\rho}\left(\frac{\partial \sigma_x}{\partial x}+\frac{\partial \tau_{xy}}{\partial y}+\frac{\partial \tau_{xz}}{\partial z}\right),\quad \frac{\partial v_y}{\partial t}=\frac{1}{\rho}\left(\frac{\partial \tau_{xy}}{\partial x}+\frac{\partial \sigma_y}{\partial y}+\frac{\partial \tau_{yz}}{\partial z}\right),\quad \frac{\partial v_z}{\partial t}=\frac{1}{\rho}\left(\frac{\partial \tau_{xz}}{\partial x}+\frac{\partial \tau_{yz}}{\partial y}+\frac{\partial \sigma_z}{\partial z}\right). \tag{11}$$

From Eq. (3), the strain rates are related to the particle velocities by the following kinematic equations

$$\begin{gathered}\frac{\partial \varepsilon_x}{\partial t}=\frac{\partial v_x}{\partial x},\quad \frac{\partial \varepsilon_y}{\partial t}=\frac{\partial v_y}{\partial y},\quad \frac{\partial \varepsilon_z}{\partial t}=\frac{\partial v_z}{\partial z},\\ \frac{\partial \gamma_{xy}}{\partial t}=\left(\frac{\partial v_y}{\partial x}+\frac{\partial v_x}{\partial y}\right),\quad \frac{\partial \gamma_{xz}}{\partial t}=\left(\frac{\partial v_z}{\partial x}+\frac{\partial v_x}{\partial z}\right),\quad \frac{\partial \gamma_{yz}}{\partial t}=\left(\frac{\partial v_z}{\partial y}+\frac{\partial v_y}{\partial z}\right).\end{gathered} \tag{12}$$

Finally, the nonlinear constitutive equations introduced in the previous sections are used to relate the stresses to the corresponding strains or strain rates.

To solve the obtained system of PDEs, complemented by the corresponding boundary and initial conditions, a staggered Chebyshev pseudo-spectral collocation is adopted, where the spatial discretization is based on a Chebyshev polynomial expansion and the time discretization is applied by explicit time integration. As a modification to the standard collocation method the field variables are located on a staggered non-equidistant grid according to Fig. 1. Here, N and $N-1$ collocation points along one distinct direction of the computational grid are defined by the Gauss-Lobatto and Gauss points (29). Applying the Chebyshev series on this grid the spatial derivatives of the field variables in Eqs. (11) and (12) are obtained. To interpolate between the two different grids a Lagrangian interpolation is applied. Furthermore, to evolve the velocities and strains in time a staggered leap frog scheme (27) is used, which is second order accurate and based on a central difference approximation of the corresponding time derivatives. According to the stability conditions, the dense meshing near the boundaries in the standard Chebyshev pseudo-spectral method leads to severe time-step restrictions. Therefore, a mapping function is used here to achieve a more equidistant node distribution and relax the time-step restriction (28). Furthermore, the spatial derivatives are determined by a direct matrix multiplication of the predefined Chebyshev difference matrices with the field variable vectors. Due to the highly parallel structure of the corresponding numerical scheme all computations are performed on the graphical processing unit (GPU) which improves the computing time considerably compared to the conventional CPU based calculations.

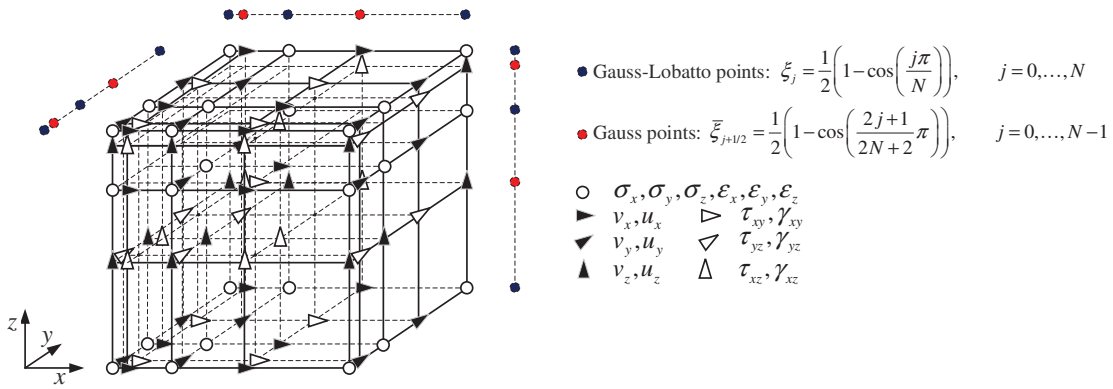

Figure 1 – Distribution of field variables at the 3-D staggered Gauss/ Gauss-Lobatto grid

The basic 3-D computational domain for the subsequent numerical simulations is illustrated in Fig. 2. Here the physical domain including the linear elastic medium with the nonlinear spherical region is surrounded by convolutional perfectly matched layers (CPML's) (30) absorbing the outgoing waves. The physical domain under consideration is excited by an ultrasonic stress source (σ_x or τ_{xy}) defined at the free y-z-plane ($x = 0$) and prescribed by the following time harmonic function

$$T\left(x=0,y,z,t\right)=\frac{1}{2}\left(A_{sig}\cdot\sin\left(2\pi f_{sig}t\right)\right)\cdot\left(1-\cos\left(2\pi\frac{t}{t_{sig}}\right)\right)\cdot H\left(t_{sig}-t\right), \tag{13}$$

where A_{sig} is the stress amplitude, f_{sig} is the excitation frequency, t_{sig} is the signal duration and H is the

Heaviside step function. To visualize and analyze the associated wave scattering problem the frequency-domain response is of particular interest and importance. For this purpose, the time-domain displacement fields of selected planes within the considered 3-D continuum are transformed to the frequency-domain by applying the fast Fourier transform (FFT). In order to separate the wave modes scattered from the nonlinear spherical region, the displacements u_x, u_y and u_z in the cartesian coordinate system (obtained from the corresponding velocities by time integration) are transformed to the spherical coordinate system (Fig. 3) as follows

$$\begin{aligned} u_r &= \sin(\theta)\cdot\cos(\varphi)\cdot u_x + \sin(\theta)\cdot\sin(\varphi)\cdot u_y + \cos(\theta)\cdot u_z, \\ u_\theta &= \cos(\theta)\cdot\cos(\varphi)\cdot u_x + \cos(\theta)\cdot\sin(\varphi)\cdot u_y - \sin(\theta)\cdot u_z, \\ u_\varphi &= -\sin(\varphi)\cdot u_x + \cos(\varphi)\cdot u_y, \end{aligned} \tag{14}$$

with the polar angle θ and the azimuthal angle φ. In Eq. (13), u_r represents the longitudinal wave mode whereas u_φ and u_θ defining the two transverse wave modes of the scattered wave field.

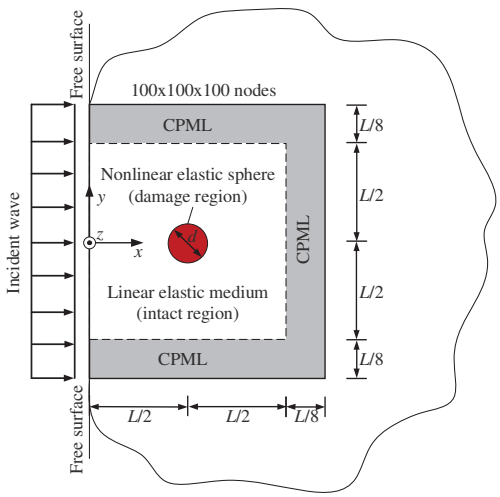

Figure 2 – 3-D Computational domain

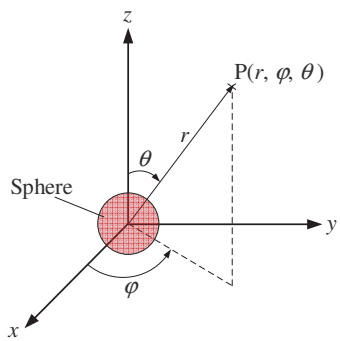

Figure 3 – Spherical coordinate system

4. NUMERICAL RESULTS AND DISCUSSION

In this section, the propagation of longitudinal and shear waves in a linear elastic medium with a localized damage region is investigated by applying the numerical method presented in the previous section. The damage region is modeled by a nonlinear elastic spherical inclusion located at the center of the computational domain inside the linear (undamaged) elastic host medium (Fig. 2). For describing the nonlinear elastic behavior, the above-mentioned nonlinear constitutive relations are separately implemented and considered. The main geometrical and material parameters used for the following numerical examples are summarized in Table 1.

Table 1 – Simulation and material parameters

L (mm)	d (mm)	A_{sig} (MPa)	f_{sig} (kHz)	t_{sig} (μs)	λ (GPa)	μ (GPa)	ρ (kg/m³)
20.00	2.00	– 31.05	100	60	9.75	15.00	2350

4.1 Quadratic nonlinear elastic case

Harmonic generation in a quadratic nonlinear elastic medium is mainly associated with a pronounced second harmonic wave field. Therefore, in this section only this second harmonic part of the total scattered wave field will be considered. The third-order elastic constants are taken as $l = m = n = -2000$ GPa. For the case of a longitudinal wave excitation (σ_x) the scattered longitudinal

part of the second harmonic wave field is characterized by two main forward and backward scattered lobes (Fig. 4a)). The scattered second harmonic wave field of both shear wave modes u_φ (Fig. 5b)) and u_θ (Fig. 5c)) shows four main lobes of nearly equal amplitude scattered in diagonal directions. In Fig. 6, the spatial distribution of the scattered second harmonic wave field generated by a primary shear wave (τ_{xy}) is illustrated. Here, a scattered second harmonic longitudinal wave field is generated (Fig. 5a)) with a homogeneous distribution around the entire circumference of the sphere. The scattered harmonic shear wave field is solely composed of the wave mode u_θ (Fig. 5b)), consisting of four nearly even lobes with a diagonal orientation. The weakly pronounced shear wave mode u_φ, inside the sphere (Fig. 5c)) can be interpreted as a non-propagating mode and does not contribute to the overall harmonic wave scattering. The basic observations and results in this section are in good agreement with the corresponding analytical solutions according to (22-24).

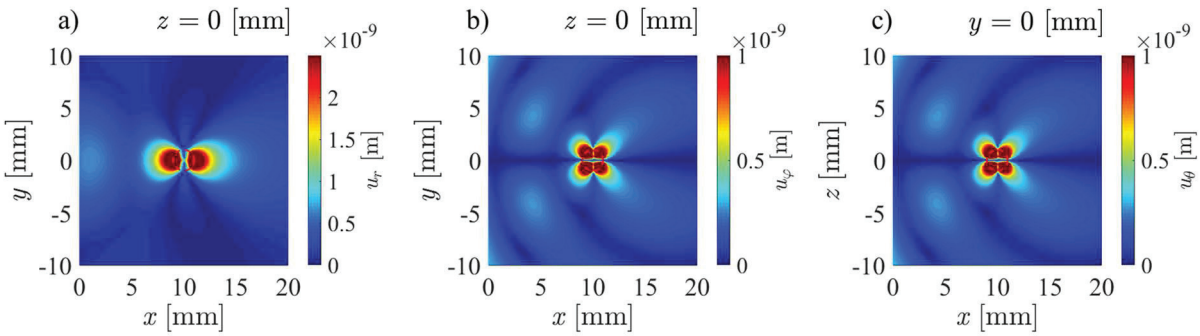

Figure 4 – Quadratic nonlinear elastic case: Scattered second harmonic wave field (f = 200 kHz) for longitudinal excitation: (a) scattered longitudinal wave field u_r and (b-c) scattered shear wave fields u_φ, u_θ

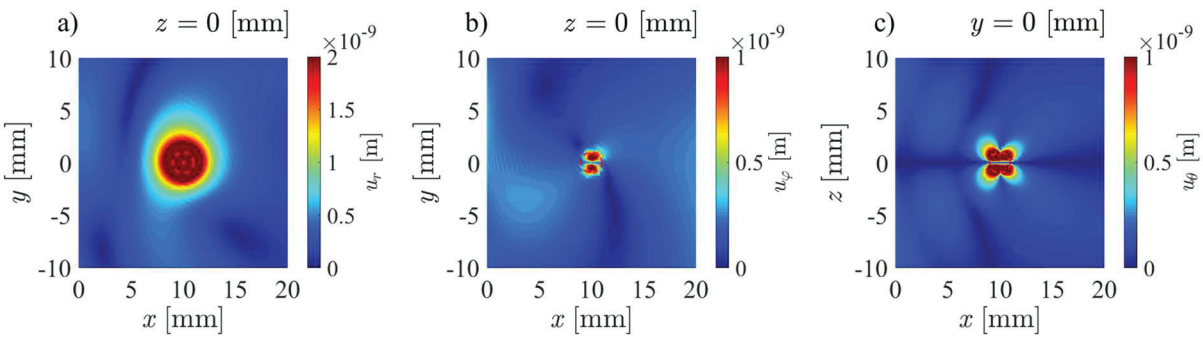

Figure 5 – Quadratic nonlinear elastic case: Scattered second harmonic wave field (f = 200 kHz) for shear wave excitation: (a) scattered longitudinal wave field u_r and (b-c) scattered shear wave fields u_φ, u_θ

4.2 Hysteretic nonlinear elastic case

For the hysteretic nonlinear case a pronounced third harmonic wave field is generated and subsequently investigated. The hysteretic parameters for the Nazarov-hysteresis model are chosen as $\gamma_1 = \gamma_2 = \gamma_3 = \gamma_4 = 300$ and $n_N = 2$. The corresponding hysteretic nonlinear constitutive relations are applied for all six independent eigensystems simultaneously according to Eqs. (12)-(15). As in the previous case the scattered harmonic wave fields for longitudinal and shear waves are presented for selected planes (Figs. 6 and 7). For a longitudinal excitation the scattered third harmonic longitudinal wave field is composed of a pronounced dipole along the x-direction and a less intensive dipole in y-direction (Fig. 6a)). Furthermore, two scattered third harmonic shear wave fields u_φ and u_θ are generated, which are characterized by four diagonal orientated lobes (Figs. 6b) and 6c)). The scattered harmonic wave fields for a shear wave excitation are illustrated in Fig. 7. In this case, the scattered third harmonic wave field of the longitudinal mode is again characterized by four diagonal orientated lobes of nearly equal magnitudes (Fig. 7a)). Considering the scattered harmonic shear wave fields in should be noted here that only the shear wave mode u_φ with the particle motion along the direction of the azimuthal angle is generated (Fig. 7b)) and the shear wave mode u_θ vanishes (Fig. 7c)). This fact

can be explained by the polarization of the corresponding incident shear wave in this example. The scattered shear wave mode is dependent on the corresponding incident shear wave mode.

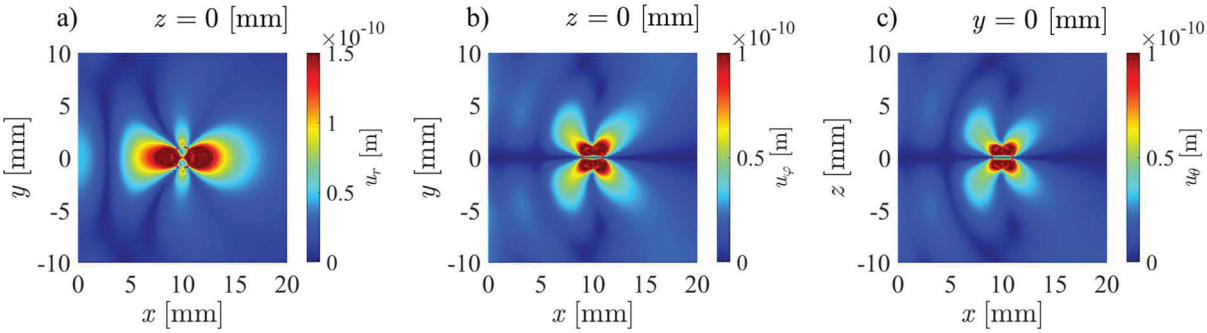

Figure 6 – Hysteretic nonlinear elastic case: Scattered third harmonic wave field (f = 300 kHz) for longitudinal excitation: (a) scattered longitudinal wave field u_r and (b-c) scattered shear wave fields u_φ, u_θ

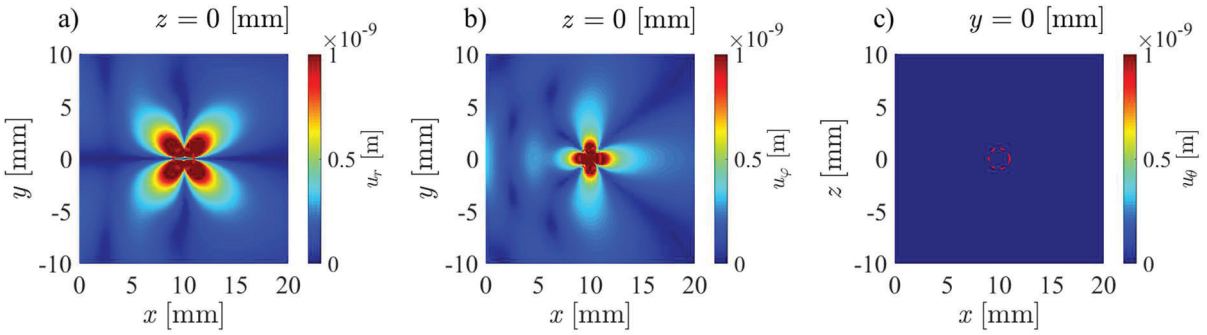

Figure 7 – Hysteretic nonlinear elastic case: Scattered third harmonic wave field (f = 300 kHz) for shear wave excitation: (a) scattered longitudinal wave field u_r and (b-c) scattered shear wave fields u_φ, u_θ

5. CONCLUSIONS AND OUTLOOK

In this study, the 3-D wave propagation in a linear elastic medium with a localized damage zone modeled by a nonlinear elastic spherical inclusion is numerically investigated. The scattered harmonic wave fields for the case of a classical quadratic nonlinear damage region and a non-classical hysteretic nonlinear damage region are analyzed. The results show that the present time-domain numerical method and the corresponding frequency-domain analysis are well suited for investigating the main characteristics of this specific nonlinear wave scattering problem. For both nonlinear material models a scattered longitudinal harmonic wave is generated independent of the exciting or incident wave mode, while the scattered second harmonic shear wave field is dependent on the nonlinear constitutive equations and the incident wave mode. In both nonlinear elastic cases, a characteristic shape of the scattered harmonic wave field is observed. This work provides an efficient and accurate tool for the numerical simulation or validation of analytical solutions regarding different inclusion shapes or different nonlinear elastic constitutive equations. Furthermore, it can be used to simulate and interpret nonlinear ultrasonic experiments for the detection and characterization of localized damages.

REFERENCES

1. Murnaghan FD. Finite deformations of an elastic solid. American Journal of Mathematics 1937;59:235.
2. Truesdell C, Toupin R. The classical field theories. In: Flügge S, editor. Principles of classical mechanics and field theory / Prinzipien der Klassischen Mechanik und Feldtheorie, Berlin, Heidelberg: Springer Berlin Heidelberg; 1960, pp. 226–858.
3. Landau LD, Lifshitz EM. Theory of Elasticity. Elsevier; 1986.
4. Haupert S, Renaud G, Rivière J, Talmant M, Johnson PA, Laugier P. High-accuracy acoustic detection of nonclassical component of material nonlinearity. The Journal of the Acoustical Society of America 2011;130:2654–61.

5. Ostrovsky L, Johnson PA.. Dynamic nonlinear elasticity in geomaterials. Nuovo Cimento Rivista Serie 24; 2001
6. Guyer RA, Johnson PA. Nonlinear mesoscopic elasticity: Evidence for a new class of materials. Physics Today 1999;52:30–6.
7. Delsanto PP, editor. Universality of Nonclassical Nonlinearity. New York, NY: Springer New York; 2006.
8. Hughes DS, Kelly JL. Second-order elastic deformation of solids. Phys Rev 1953;92:1145–9.
9. Egle DM, Bray DE. Measurement of acoustoelastic and third-order elastic constants for rail steel. The Journal of the Acoustical Society of America 1976;60:741–4.
10. Shokouhi P, Rivière J, Lake CR, Le Bas P-Y, Ulrich TJ. Dynamic acousto-elastic testing of concrete with a coda-wave probe: Comparison with standard linear and nonlinear ultrasonic techniques. Ultrasonics 2017;81:59–65.
11. Renaud G, Talmant M, Marrelec G. Microstrain-level measurement of third-order elastic constants applying dynamic acousto-elastic testing. Journal of Applied Physics 2016;120:135102.
12. Breazeale MA, Thompson DO. Finite-amplitude ultrasonic waves in aluminum. Applied Physical Letters 1963;3:77–8.
13. Thompson RB. Higher harmonics of finite amplitude ultrasonic waves in solids. The Journal of the Acoustical Society of America 1976;59:1087.
14. Matlack KH, Kim J-Y, Jacobs LJ, Qu J. Review of second harmonic generation measurement techniques for material state determination in metals. Journal of Nondestructive Evaluation 2015;34:273.
15. Shah AA, Ribakov Y, Zhang Ch. Efficiency and sensitivity of linear and non-linear ultrasonics to identifying micro and macro-scale defects in concrete. Materials & Design 2013;50:905–16.
16. Berndt TP, Green RE. Feasibility study of a nonlinear ultrasonic technique to evaluate adhesive bonds. In: Green RE, editor. Nondestructive Characterization of Materials VIII, Boston, MA: Springer US; 1998, p. 125–31.
17. Hikata A, Chick BB, Elbaum C. Dislocation contribution to the second harmonic generation of ultrasonic waves. Journal of Applied Physics 1965;36:229–36.
18. Kim J-Y, Jacobs LJ, Qu J, Littles JW. Experimental characterization of fatigue damage in a nickel-base superalloy using nonlinear ultrasonic waves. The Journal of the Acoustical Society of America 2006;120:1266–73.
19. Liu M, Tang G, Jacobs LJ, Qu J. Measuring acoustic nonlinearity parameter using collinear wave mixing. Journal of Applied Physics 2012;112:024908.
20. Küchler S, Meurer T, Jacobs LJ, Qu J. Two-dimensional wave propagation in an elastic half-space with quadratic nonlinearity: A numerical study. The Journal of the Acoustical Society of America 2009;125:1293–301.
21. Xu H, Day SM, Minster J-BH. Hysteresis and two-dimensional nonlinear wave propagation in Berea sandstone. Journal of Geophysical Research 2000;105:6163–75.
22. Tang G, Jacobs LJ, Qu J. Wave scattering by an elastic inclusion with quadratic nonlinearity, Burlington, VT: 2012, p. 269–76.
23. Tang G, Jacobs LJ, Qu J. Scattering of time-harmonic elastic waves by an elastic inclusion with quadratic nonlinearity. The Journal of the Acoustical Society of America 2012;131:2570–8.
24. Kube CM. Scattering of harmonic waves from a nonlinear elastic inclusion. The Journal of the Acoustical Society of America 2017;141:4756–67.
25. Nazarov VE, Radostin AV, Ostrovsky LA, Soustova IA. Wave processes in media with hysteretic nonlinearity. Part I. Acoustical Physics 2003;49:344–53.
26. Helbig K. A formalism for the consistent description of non-linear elasticity of anisotropic media. Revue de l'Institut Français du Pétrole 1998;53:693–708.
27. Vanaverbeke S, Abeele KVD. Two-dimensional modeling of wave propagation in materials with hysteretic nonlinearity. The Journal of the Acoustical Society of America 2007;122:58–72.
28. Kosloff D, Tal-Ezer H. A modified Chebyshev pseudospectral method with an O(N-1) time step restriction. Journal of Computational Physics 1993;104:457–69.
29. Kopriva DA, Kolias JH. A conservative staggered-grid Chebyshev multidomain method for compressible flows. Journal of Computational Physics 1996;125:244–61.
30. Drossaert FH, Giannopoulos A. Complex frequency shifted convolution PML for FDTD modelling of elastic waves. Wave Motion 2007;44:593–604.